ACTIVE CONTROL OF COMBUSTOR PROCESSES

B. T. Zinn*, M. G. Allen, A. Glezer, J. I. Jagoda, Y. Neumeier and J. M. Seitzman
Schools of Aerospace, Mechanical and Electrical and Computer Engineering
270 Ferst Drive
Georgia Institute of Technology
Atlanta, GA 30332-0150, USA

Abstract

This paper describes results of several studies of sensors, actuators and control systems for active control of combustor processes. First, the paper discusses the performance of an adaptive active control system (ACS) for controlling detrimental combustion instabilities. This ACS consists of an observer that determines the time dependent characteristics of the instability in real time, a adaptive controller and a fuel injector actuator. During control, the controller sends a time varying signal to the actuator and the corresponding system's response is determined by the observer in practically real time. These data are then used to determine the optimum control parameters. Results obtained in several studies demonstrate that this ACS can rapidly and effectively damp combustion instabilities without apriori knowledge of the characteristics of the instability.

The second part of the paper discusses two open loop applications of synthetic jets (SJ) aimed to improve combustor mixing processes. Specifically, the paper describes studies whose objective was to improve the mixing between fuel and air and the combustor pattern factor. The results of these studies show that both improvements are possible. These studies also show that SJ can be used to enhance both small and large scale mixing processes and that they significantly improve the pattern factor.

The third part describes a study of the possibility of using an internally mixed fuel atomizer to control the spray characteristics; i.e., independently control the spray's flow rate and mean droplet diameter. Results of experimental and theoretical studies show that by controlling the supply pressures of the air and fuel streams it is possible to independently vary the spray's mean diameter while keeping the fuel flow rate constant and vice versa.

The last part of the paper discusses the development of a wireless, MEMS scale, pressure transducer for high temperature applications; e.g., gas turbines compressors and combustors. The developed pressure transducer is constructed of high temperature ceramic liners that are used in electronic packaging. Using appropriate construction, a cavity is formed between two external liners, resulting in a device that behaves as a capacitor. The capacitor is connected to an inductor that is "deposited" on one of its external liners to form an LC circuit with a specific resonant frequency. When a change in pressure deforms one (or both) of the external liners, the system's capacitance and, thus, resonant frequency change. This frequency change is sensed by an "external" antenna and is "related" to the pressure change, thus providing means for determining the pressure and its wireless transmission.

*Corresponding author; David S. Lewis Jr. Chair and Regents' Professor, Schools of Aerospace and Mechanical Engineering

Introduction

This paper presents the findings of several studies on active control of combustion processes that are being performed at Georgia Tech under several government-sponsored programs. Specifically, this paper discusses: 1) active control of combustion instabilities in rocket motor and gas turbine combustors, 2) application of SJ in active control of mixing processes and the pattern factor in gas turbine combustors, 3) a "smart" fuel injector for controlling combustion processes, and 4) a MEMS, wireless, pressure sensor for gas turbines and related applications. These active control studies were stimulated by 1) the realization that active control systems (ACS) may offer the only or the most rational approach for attaining certain propulsion systems performance goals and 2) recent improvements in computer hardware and software, microelectronics, actuators, sensors and control approaches that provide the capabilities needed for developing advanced ACS for the next generation of propulsion systems. Examples of combustor phenomena that may be controllable using with ACS include combustion instabilities, flame holding, emissions, combustion efficiency and combustor pattern factor. Additionally, ACS could potentially improve engine reliability by, e.g., improved health monitoring and prognostication, and compensating for problems caused by design shortcomings, component failure and aging.

ACS for propulsion systems and gas turbines generally operate in a closed loop and consist of one or more sensors, a controller and one or more actuators. The sensors measure data, e.g., pressures, temperatures, or concentrations. These data are used by the controller to determine the state of the system and generate control signals for the actuators, whose role is to modify the system's operation in a desired way. To meet the expected demands of future ACS, ongoing studies aim to develop advanced sensors, actuators, control approaches and computer hardware and software that will provide capabilities for operation with a wide bandwidth and control of complex phenomena that are not controllable with state of the art technologies. To be practical, the developed ACS will have to be lightweight, integratable with the engine's hardware and control system, and exhibit robustness that will allow them to survive in the harsh engine environment over a long period of time. The remainder of this paper presents results of studies that were undertaken to meet these goals.

Paper presented at the RTO AVT Symposium on "Active Control Technology for Enhanced Performance Operational Capabilities of Military Aircraft, Land Vehicles and Sea Vehicles", held in Braunschweig, Germany, 8-11 May 2000, and published in RTO MP-051.

Active Control of Combustion Instabilities

Combustion instability occurs when a periodic combustion process excites large amplitude oscillations of one or more natural acoustic modes of the combustor[1,2]. Such an instability may be driven by one or more feedback mechanisms that involve interactions between, e.g., acoustic oscillations in the combustor and flow rate oscillations in the air and/or fuel supply, and combustion in vortices and/or shear layers. These feedback mechanisms drive acoustic oscillations when the magnitude of the phase difference between the heat release and pressure oscillations is smaller than ninety degrees[1]. Combustion instability occurs when the driving by the oscillating combustion process is larger than the acoustic damping by, e.g., viscous processes, acoustic liners and acoustic energy radiation out of the combustor. An instability generally starts as a small amplitude oscillation whose amplitude grows exponentially in time until it stabilizes at some constant amplitude, limit cycle, oscillation. Combustion instabilities are undesirable because they generally increase the mechanical loads on the combustor wall and engine components, excite vibrations in various components and significantly increase convective heat transfer rates to the combustor wall and adjacent components. Alone or in combination, these phenomena shorten component life and can cause catastrophic engine failure.

Until recently, passive approaches were used to control combustion instabilities[2]. These often consisted of changing the combustor design and/or operating conditions in an effort to decrease the combustion process driving and/or increase the damping of the excited acoustic modes, and prevent amplification of unstable acoustic modes. These changes included, e.g., modifications of the reactants injection systems to make them less responsive to combustor disturbances, elimination of sharp corners and "sudden" area changes to minimize shear layer formation and, thus, periodic combustion in vortices, changing fuel properties, and the addition of damping devices, e.g., acoustic liners, to increase the system's acoustic damping. Unfortunately, due to inadequate understanding of the damping and driving processes, development of passive control approaches often required lengthy and costly research and development programs that did not produce satisfactory results. Furthermore, passive control approaches that worked well in one system have, on occasion, reduced combustor stability when applied to another system, thus clearly demonstrating the lack of understanding and shortcomings of passive control approaches.

The persistent appearance of combustion instabilities in a wide variety of combustors and the inability to "design" them out of the system or rapidly damp them after their unexpected excitation stimulated efforts to develop ACS for unstable combustors in the early 1980s. Since most of these efforts are discussed in several review articles[1,3,4], the discussion of this subject matter in this paper will focus on the ACS developed at Georgia Tech[1,5]. These efforts started with the development of an ACS for unstable liquid rockets and subsequently demonstrated that the developed ACS can also control combustion instabilities in gas turbine combustors. The goal of the Ga. Tech studies was to develop a practical ACS that could rapidly damp large amplitude, nonlinear, high frequency combustor oscillations whose characteristics are not known a priori. To meet this goal, the developed ACS needed capabilities for 1) determining the unknown, (possibly) time varying, characteristics of the instability; i.e., the amplitudes, frequencies and phases of several combustor modes, in real time, 2) determining the control signals needed to damp one or more unstable combustor modes, 3) providing large actuation, and 4) damping high frequency oscillations.

The original ACS developed to meet these goals is shown in Fig. 1. It consists of a pressure sensor, an observer, a controller and a fuel injector actuator. The sensor measures the combustor pressure and sends its output to the observer, which analyzes the measured pressure to determine the amplitudes, frequencies and phases of the unstable combustor modes in practically real-time. The observer's output is then sent to the controller where the required control signal for the modes of interest are either determined adaptively[6] or with the aid of data measured in open loop combustor controllability tests[1,5]. The generated control signals (for different modes) are then synthesized into a time dependent control signal that is sent to the fuel injector actuator. The latter modulates the injection rate of a secondary fuel stream to generate heat release oscillations within the combustor that are out of phase with the unstable pressure oscillations and, thus, rapidly damp the combustion instability.

The development of this ACS was guided by the knowledge, based upon Rayleigh's criterion[1], that heat addition oscillations damp acoustic pressure oscillations when the two are out of phase. Thus, it was assumed that the instability consists of a number of independent modes whose amplitudes, frequencies and phases are not known a priori, and may change with time. To damp such an instability, it was necessary for the ACS to track the characteristics of each unstable mode in real time, generate a control signal for damping each mode separately, and modulate the injection rate of the secondary fuel stream at the frequency of each unstable mode with the appropriate amplitude and a phase delay.

Initially, an attempt was made to use FFT to analyze the measured pressure signal. When the FFT failed to accomplish this in real time, an observer "algorithm" was developed[7]. This algorithm assumes that the measured combustor pressure $P_m(t)$ can be expressed in the following Fourier-like series:

$$P_m(t) = \sum_{n=1}^{N} \left[a_n(t) \sin(\varpi_n(t)t) + b_n(t) \cos(\omega_n(t)t) \right] \quad (1)$$

whose frequencies $\omega_n(t)$ and amplitudes $a_n(t)$ and $b_n(t)$ are unknown, and may be time dependent. These unknowns are determined in an iterative procedure that starts with an assumed value of the unknown frequency $\omega_n(t)$ and rapidly converges to the correct values of the unknown coefficients $\hat{a}$ and $\hat{b}$ and the frequency $\hat{\omega}$[7]. This procedure first determines the characteristics of the mode with the largest amplitude. Once this mode has been identified, it is "subtracted" from the measured signal P_m, see Eq. 1, and the above described procedure is applied to the resulting signal to determine the amplitude, phase and frequency of

the largest amplitude mode in the "remaining" signal. This procedure is repeated until the characteristics of a desired number of modes are determined. An alternate procedure for simultaneous determination of the characteristics of a number of modes is described in Ref. 7. Fortunately, results obtained to date strongly suggest that successful damping of an instability may only require identification and active damping of one or two unstable modes, which can be accomplished by this observer in practically real-time.

Another important contribution of this program was the development of a unique fuel injector actuator that can modulate the flow rate of the "control" fuel stream over a large frequency range. It uses a magneto-strictive actuator, i.e., Terfenol D, which changes its length in response to changes in the intensity of an imposed magnetic field. The latter is controlled by the electric current in a coil that is wound around the actuator. As the length of the actuator varies, it changes the cross sectional area in the flow path of the "controlled" fuel stream into the combustor, thus changing the flow rate of this fuel stream in a desired manner by effectively opening and closing a fuel valve. To date, fuel injector actuators were developed and operated that are capable of modulating the flow of gaseous fuels over a 0-2000 Hz frequency range[5] and liquid fuels over a 0-3000 Hz range[8]. Since the upper limits of these frequency ranges are considerably higher than those of any other known fuel injector, these fuel injector actuators provide the propulsion community with capabilities for controlling high frequency combustion instabilities.

Typical performance of this ACS while actively (and adaptively) controlling a large amplitude, 100 Hz instability is shown in Fig. 2. For the first two seconds of this test, the pressure oscillations in the combustor are uncontrolled, oscillating with a limit cycle amplitude of over 2psi. After two seconds, an algorithm to automatically identify the proper control phase is invoked. This identification process permits control without costly open loop testing that is typically required for closed-loop active control. In this case, the identification process spans two seconds, and then control is applied. When the control is activated, the unstable pressure oscillations are reduced by approximately 15dB within ten cycles, or 100 milliseconds[6]. Similar performance was demonstrated on small and large-scale low NOx gas turbine combustors, at atmospheric and high pressure test conditions.

In summary, the above-discussed research has clearly demonstrated that ACS potentially offers a very promising approach for controlling combustion instabilities in propulsion systems and gas turbines.

Synthetic Jet Actuators for Combustor Mixing and Pattern Factor Control

This section describes the application of synthetic jets (SJ) to improve combustor mixing processes and, thus, combustor performance. For example, poor mixing in gas turbine combustors can produce a non-uniform distribution of equivalence ratio, which, in turn, may increase emissions and specific fuel consumption. Mixing problems can likewise lead to "hot" spots at the turbine inlet and increase the likelihood of combustion instabilities. Inefficient mixing may also extend the combustion process into the turbine, resulting in an unacceptable operating condition.

SJ[9] may offer an attractive approach for controlling combustor mixing processes through open or closed loop excitation of large and/or small-scale structures in the combustor flow. A schematic of a SJ actuator is shown in Fig. 3. It consists of a cavity whose lower wall is a membrane that is oscillated at a desired frequency by, e.g., a piezoelectric transducer. The cavity is connected to the flow above by a small orifice. As the membrane moves downward during the first half of the cycle, the cavity's pressure decreases and gases from all directions flow into the cavity (in a "sink-like" manner). As the membrane moves upward during the second half of the cycle, the gases that entered the cavity earlier are ejected as vortex rings (in axisymmetric SJ). The membrane is often driven at a resonant frequency of the actuator to maximize the strength of the generated vortices. Continuous operation of the actuator forms a train of vortical structures that coalesce into a SJ. The vortical structures that synthesize each SJ scale with the oscillation frequency of the cavity's membrane and can be adjusted to match, and directly interact with, small-scale eddies within the equilibrium range of the embedding shear flow. Large-scale flow structures and global entrainment away from the cavity are affected by amplitude modulation of the membrane's excitation waveform.

This section describes studies that are concerned with two potential applications of SJ in the control of combustor mixing processes. The first involves installation of SJ in the fuel injector to improve the mixing of fuel and air, especially under extreme conditions where passive mixing techniques fail. An example would be high altitude relight conditions, when there is little airflow, and devices such as swirlers do not produce rapid fuel-air mixing. A second goal is to gain control authority over the spatial distribution of fuel in the combustor, which may be needed to compensate, for example, for fuel injector problems.

The second study involves the use of SJ to control the temperature profile at the combustor exit. Detailed tailoring of pattern factors in the flow entering turbines in future turbine engines is gaining importance because of the higher temperatures of the combustion products leaving the combustor. At the same time, as permissible turbine entrance conditions approach stoichiometric flame temperatures, less dilution air is available to enhance mixing. Therefore, alternative techniques have to be found to replace the mixing effects of cross flow jets of cold, high pressure air from the compressor, which are currently used to enhance mixing downstream of the combustor.

Fuel-Air Mixing:

The present work focuses on mixing enhancement between coaxial round jets. The traditional approach to small-scale mixing enhancement in such free shear flows has been *indirect* and has relied primarily on the manipulation of large-scale, global instability modes of the base flow upstream of mixing transition. More efficient control of mixing in fully turbulent shear flows might be achieved by direct (rather than hierarchical) control of both the large-scale entrainment *and* the small-scale mixing processes. The present work focuses on mixing enhancement based on concurrent manipulation of *both* the small- and large-scale dynamical processes and the coupling between the large- and

small-scale motions in the shear and mixing layers of the coaxial round jets.

Two similar experimental systems, one focusing on velocity measurements and the other on scalar mixing, have been developed to ascertain the efficacy of the SJ. In both experiments, the outer boundary of the annular jet is 2.54 cm in diameter, while the inner air jet is produced with a 1.4 cm diameter central tube having 1 mm wall thickness. This yields an inner/outer flow area ratio of 0.5. In the velocity facility, a nozzle having a contraction ratio of 36:1 forms the outer boundary of the annular flow. In the mixing facility, the outer boundary of the annular jet is formed by a simple 2.54 cm diameter tube, and the annular gas stream is acetone seeded into air (~23% acetone by volume). Three inner/outer velocity ratios (nominally 0.35, 0.65, and 1.4) have been investigated, with some results for $U_I / U_o = 0.65$ presented here. The total volume flow rate of the combined jets is nominally constant, and is equivalent to a uniform jet issuing out of the combined flow area $A_o + A_i$ at 11 m/s (Re_{DH} = 7700 based on the hydraulic diameter). Nine individually controlled actuators, equally spaced around the outer circumference of the main flow, produce SJ. Each SJ issues from a rectangular, arc-shaped orifice having a width and length of 0.5 and 9 mm, respectively. The carrier waveform of the actuators is nominally 1.2 kHz (near their resonant frequency), and the amplitude, duty cycle, and relative phase of each of the modulating waveforms of the individual actuators are computer controlled. The flow mechanisms induced by the excitation are inferred from detailed phase-locked measurements of the velocity field using two-component hot wire anemometry, and the resultant mixing of a passive scalar is studied using planar laser-induced fluorescence (PLIF) of the acetone seeded into the annular jet.

The power spectra of the streamwise velocity at the radial location where $U(x,r)/U_{max}(x) = 0.5$ for $U_I / U_o = 0.65$ are shown in Figs. 4a and b for high frequency forcing only and pulse-modulated forcing, respectively. The corresponding spectral distributions of the unforced flow are also shown for reference in each figure. The flow scales that are introduced by the forcing are apparent in the figure. High frequency forcing results in spectral peaks at the forcing frequency (1180 Hz) and some of its higher harmonics. The amplitude of the spectral peak at the forcing frequency decreases with downstream distance, but is still discernible compared to the background flow, even at $x / D_o = 5$. Amplitude modulation of the excitation waveform, with a modified square wave, results in spectral peaks at the carrier and modulation frequencies as well as at several harmonics in the near field. At $x / D_o = 2$, the high-frequency spectral peaks correspond to the carrier forcing frequency and its sidebands. The peaks at the carrier and modulation frequencies are still discernible at $x / D_o = 5$. The regions of the spectra with slope m = -5/3 indicate that the forcing frequency is within the equilibrium range of the flow.

Cross-stream distributions of the streamwise and radial velocity components are measured in a plane that intersects the jet centerline and passes through the azimuthal center of an actuator at the edge of the jet on one side and between two actuators on the other side. The measurement domain is $x / D_o \leq 5$ with increments of $\Delta x / D_o = 0.25$ and $\Delta r / D_o = 0.025$. For the amplitude-modulated cases, data are acquired phase locked to the modulation waveform at 72 equal phase increments. Figure 5 shows raster plots of the mean streamwise velocity for $U_i / U_o = 0.65$ and $x / D \leq 3$ with all three forcing conditions. The increase in jet spreading and decrease in annular jet velocity are apparent. While the mean effect is not as dramatic with amplitude modulated forcing, the raster plot of phase-averaged streamwise velocity shows formation of well-defined large-scale structures. The effect of unmodulated excitation input on radial distributions of U, u', and V for $U_i / U_o = 0.65$ at several streamwise stations is shown in Figs. 6a,b, and c. The corresponding distributions for the unforced flow are shown for comparison using open symbols. Since the jet actuators are placed near the radial edges of the outer jet, their effect on the mean streamwise velocity is most apparent through a radial expansion of the jet flow field (more than $0.1D_o$ at $x / D_o = 0.04$). As mentioned above, the actuation is asymmetric left to right in the distributions in Fig. 6. This asymmetry is apparent at $x / D_o = 0.25$ and 1 where the jet spreads radially towards the active actuator on the right. Davis and Glezer[10] obtained similar spreading by azimuthal non-uniform forcing having a three-fold symmetry of a single jet. The forcing leads to an increase in u' throughout the entire width of the annular flow for $x / D_o < 1$ but does not increase the turbulence in the core flow. By $x / D_o = 1$, the differences between distributions of U and u' in the forced and unforced flows are reduced and by $x / D_o = 3$ the unforced and forced flows are quite similar with less turbulent intensity in the forced flow. The reduction in u' downstream with forcing is ostensibly due to increased dissipation in the near field. The radial velocity is especially significant to the mixing of the two streams because it leads to entrainment of the jets. In Fig. 6c the radial velocity away from the jet centerline is taken to be positive to the right of the centerline and vice versa on the left. The strongest effect of the forcing occurs near the jet exit plane ($x / D_o = 0.04$). In the unforced flow, the radial velocities in the core and annular flows are of opposite sign and are directed towards the wake region of the pipe wall. In the presence of forcing, the mean radial velocity in both the core and annular flows is directed outward except within the wake and near the jet actuators. This mean outward radial velocity results from the time-periodic entrainment by the SJ. Time series of the radial velocity (not shown), indicate that in the wake region of the center tube, while the mean radial velocity is nearly zero, the instantaneous velocity oscillates at the forcing frequency resulting in the formation of vortical structures in the mixing region.

The effect of actuation on mixing is seen in the images of Fig. 7, which compares, instantaneous, side view images up to $x/D_o = 3$, for the three forcing cases with $U_i/U_o = 0.62$. The intensity of each pixel is converted to a local mixture fraction (f), which is defined as the ratio of the mass of fluid that originated in the annulus at the jet exit to the total mass in a measurement volume (pixel). The unforced case (Fig. 7a) has large amounts of pure annular fluid persisting downstream. The annular fluid just begins to mix into the center of the flow at $x/D_o = 5$ (not shown). The high frequency forcing (Fig. 7b) produces an enhancement of the jet growth and a broadening of both mixing layers (between the ambient and the annular jet, and between the annular and inner jets). The annular fluid is mixed into the center of the flow more rapidly, and the regular structures visible at the

outer edge correspond to the individual pulses of the high frequency forcing. The amplitude modulation result (Fig. 7c) shows what appear to be large, coherent structures that correspond to the modulation frequency. These periodic scalar fields are convected at a velocity of the order of the mean flow.[11] The large-scale structures significantly increase the entrainment between the central jet and the annular flow, and are able to penetrate to the jet centerline within a few jet diameters.

One measure of mixing effectiveness of the SJ is the rate at which pure annular fluid becomes mixed. The axial variation of the unmixed fuel (defined as $f \geq 0.95$) for unforced and forced cases was determined from radial and azimuthal integration of data similar to that shown in Fig. 7. This comparison shows that high frequency, forcing, relative to the unforced case, greatly increases the rate at which pure fluid becomes at least partially mixed, and that amplitude modulation further increases the rate of fuel mixing. In the latter case, virtually all the pure fluid is gone as early as $x/D_o = 0.5$, while the high frequency forcing and unforced flows do not achieve this until farther downstream. The improved effectiveness of amplitude modulated forcing results from the increased entrainment produced by the large-scale structures in this case. The evolution of these structures is clearly seen in Fig. 8, which compares the velocity and mixing measurements at selected phases of the amplitude modulation.

Pattern Factor Control:

Next, the results of a study of the application of SJ in the control of pattern factor (combustor-exhaust/turbine- inlet temperature profiles) are described. It was conducted in the facility shown in Fig. 9a. It consists of a rectangular chamber (450mm x 92mm x 75 mm) with provisions for optical and probe access. Separate streams of room temperature air and combustion products from a premixed methane-air flame are introduced in parallel streams into the chamber. SJ enter through an orifice plate in the chamber floor, 145 mm downstream of the its entrance. These jets are generated by a piston in a cylinder below the orifice plate. Temperature distributions at the exit to the chamber are measured with a K-type thermocouple rake that can be translated laterally across the flow. Hot film anemometry is used to measure the SJ velocities.

The temperature stratification in the flow without actuation is clearly seen in the profile shown in Fig. 9b, where different temperature ranges are represented by gray scales. As the mixing between the layers of flow at different temperatures increases, the temperature profile becomes more uniform. This mixing is quantified using an entropy method, which utilized the fact that entropy increases with mixing. Each temperature distribution, therefore, is associated with a given level of entropy, or more precisely, an entropy difference (Δs) between the measured system and a (hypothetical) uniformly mixed system of the same average temperature. A fractional improvement in mixing (ζ) is then defined as the difference between Δs without actuation and that with actuation, as a fraction of the non-actuated Δs. Thus, ζ varies between 0 and 1, and increases as the mixing enhancement by the SJ improves.

Tests to date have shown that mixing can be very significantly enhanced with the SJ[12]. This enhancement increases with the degree of actuation, measured as the ratio between the *peak* velocity from the SJ and the mean velocity of the main flow, see Fig. 10. Mixing improves once the jet velocity exceeds twice the main flow speed and the effect levels off (at a nearly uniform composition) when that ratio reaches ten. So far, changes in frequency (from 2 to 30 Hz) appear to have no effect on mixing. Furthermore, test with plates having different orifices, such as rows of circular orifices and long narrow slots of same total aperture areas have shown that mixing is only weakly dependent on actuator orifice shapes or orientation (crosswise vs. streamwise relative to the flow).

The mechanism by which these relatively small SJ can so significantly affect the temperature distribution in the much larger main flow is currently being investigated. High speed shadowgraphy is being utilized to visualize the interaction between the SJ and the main flow. Mie scattering techniques are planned to quantify the local degree of mixing between hot and cold flow in the region where SJ and main flow interact, and planar laser-induced fluorescence of acetone injected into the actuators will be used to measure the degree of dissipation of the synthetic jet flow into the main stream.

Internally Mixed Liquid Atomizer for Active Control of Spray Characteristics

The quality of combustion processes, e.g. ignition, flame stability, efficiency and emissions, in liquid fueled engines, strongly depends on the atomization quality[13]. There is evidence that the characteristics of the combustion process for a given operating condition may be optimized by burning a spray that is characterized by a specific droplet size, which may not be the droplet size generated by the injector. For example, Rink and Lefebvre[14] report that fine atomization causes a decrease in the production of unburned hydrocarbon because of the reduction in evaporation time. This, in turn, increases the time available for NO reactions in the post flame region to proceed towards equilibrium, thus increasing NO_x emissions. These and related studies strongly suggest that a combustor's performance could be optimized by using fuel atomizers that could be controlled to produce sprays with desired properties.

The objective of the research described in this section is to develop a fuel atomizer that could be actively controlled to provide a fuel spray with desired properties over a wide range of operating conditions of airborne gas turbines. Such an injector would overcome the shortcomings of the state-of-the-art pressure and air-blast atomizers that produce poor sprays during some operating conditions; e.g., startup and idling. Furthermore, active control of fuel droplet size at any desired fuel flow rate during a flight can be used to control UHC, NOx and CO emissions.

A schematic of the investigated internally mixed atomizer is shown in Fig. 11. Liquid fuel is axially supplied to the atomizer at its upstream end and air is injected through series of holes symmetrically distributed around the injector's periphery downstream of the liquid entry point. As the air expands within the injector and occupies an increased fraction of the available cross sectional area, the cross

sectional area available to the liquid is reduced. This is accompanied by acceleration of the liquid phase and, thus, an increase in its kinetic energy, which leads to liquid atomization. Also, the relative motion between the phases produces shear forces at their interfaces that "strip" liquid droplets from liquid ligaments, resulting in further liquid atomization. Together, these processes produce a mixture of liquid ligaments and droplets and air inside the injector[15].

The performance of the developed injector has been investigated in an experimental setup specifically developed for this purpose. It consists of a vessel, with windows, that can be operated over a wide range of pressures. The injector is installed at the top of the vessel and the injected liquid is collected at the bottom. The windows provide optical access for determining the properties of the spray. To date, series of tests were conducted to determine the dependence of the spray properties upon the amount of atomizing air, the liquid supply pressure and the test chamber pressure[15]. This study also sought to determine the mode of operation that would permit control of the characteristics of the generated spray.

A performance map of the investigated injector is shown in Fig. 12. It shows the dependence of the Sauter Mean Diameter (SMD) of the generated spray upon the liquid flow rate and supply pressure. It should be noted that in these experiments the liquid flow rate was controlled by varying the flow rate of atomizing air. The data in Fig. 12 show that by varying the liquid supply pressure while keeping the liquid flow rate constant, i.e., moving along the vertical line in Fig. 12, which requires variation of the air flow rate, one can vary the droplet sizes while keeping the liquid flow rate constant. Figure 12 also shows that simultaneously changing the liquid supply pressure and flow rate (again, by varying airflow rate) while moving along the horizontal line in Fig. 12 permits operation with a constant droplet size over a range of liquid flow rates. Thus, for a given combustor pressure, the injector's performance can be controlled by changing the airflow rate and the liquid supply pressure simultaneously[15].

In parallel efforts, a model for predicting the performance of the above-described injector is being developed. The objective of this study is to develop an analytical tool that could be applied in the design of improved internally mixed injectors and to predict the injector's flow and spray characteristics, e.g., the liquid flow rate and mean droplet size, under different operating conditions. The developed two phase flow model assumes that the flow is one-dimensional, wall friction is negligible, the liquid flow is isothermal incompressible, the flows are uniform and steady and the air behaves as a perfect gas. Also, the airflow injection ports are approximated by an annular slit of a finite width at the injector's wall. Finally, it has been also assumed that as the two phase flow evolves the liquid break ups into droplets in a manner that maintains the local Weber number ($We = \rho_a V_r^2 D/\sigma$; i.e., the ratio of the inertial and surface forces) at a value of 10 and that the droplets do not coalesce to form larger droplets[16].

The system of equations governing the two-phase flow in the injector's passage are the air mass conservation, liquid mass conservation, combined air and liquid momentum conservation, combined air and liquid energy conservation and liquid energy conservation. The interaction between the phases, which appears only in the liquid energy equation, is modeled as a drag force acting on the liquid. These equations are solved numerically to determine various flow and spray properties inside the injector[16].

Figure 13 compares the predictions of the model with measured data. Figure 13a shows that the measured and predicted liquid flow rates are in good agreement, while Fig. 13b shows that measured and predicted mean droplet diameters are in good qualitative agreement[16].

In summary, the results obtained to date strongly suggest that the developed, internally mixed, atomizer can be used to control fuel spray properties. Such control can be attained by simultaneously varying the liquid supply pressure and air flow rate. It has also been shown that a developed theoretical model reasonably predicts the injector's performance.

High Temperature Ceramic Pressure Sensors

Micromachined silicon pressure sensors are widely utilized in industry. In general, the pressure sensor design is based on a flexible silicon membrane as the sensing element, coupled with silicon piezoresistors or a capacitive structure and silicon circuitry for data retrieval. These sensors are well developed and have been documented extensively in the literature[19]. However, micromachined silicon sensors are typically subject to operating temperature limitations due to a variety of factors, including piezoresistive temperature sensitivity and the poor mechanical properties of silicon at higher temperatures. Thus, applications such as sensing pressure in turbine engine compressors require development of other types of sensors that offer high temperature stability.

In the literature, potential high-temperature materials have been investigated as an alternative to silicon processing. Silicon carbide, polycrystalline diamond and ceramic materials have been reported as high-temperature materials for sensor fabrication[20,21]. Silicon carbide pressure sensors employ the flexible membrane design and use piezoresistors to measure pressure changes. Silicon carbide circuitry is also possible to retrieve the pressure data. Polycrystalline diamond pressure sensors also employ a flexible membrane and piezoresistors. These technologies show great promise for integrated high temperature pressure sensors, but their manufacturing infrastructure is not nearly as well developed as that for silicon and electronic packages for silicon.

The microelectronics packaging industry offers a well-developed ceramic packaging procedure using ceramic co-fireable tape. The ceramic tape consists of alumina particles and glass particles suspended in an organic binder, which is subsequently fired to form a ceramic structure. In general, this type of tape is referred to as low temperature co-fireable ceramic (LTCC) because the curing (firing) temperature is only 900°C[22]. Ceramic tapes made solely from alumina particles are also available and have curing temperatures above 1600°C. Besides high temperature stability, the co-fired ceramic tape has good mechanical properties that allow membrane designs similar to those of the silicon pressure sensors. From our investigations, the ceramic tape is an excellent choice for the fabrication of pressure sensors for high temperatures. By incorporating a passive wireless readout technology with the sensors[23], it is possible to also circumvent the issues associated with contacts and wired connections in a high temperature environment. The focus of this study has been to develop such a sensor for turbine compressor pressure sensing.

A schematic of the wireless pressure sensor concept is shown in Fig. 14. The sensor consists of a sealed cavity, ideally containing vacuum, on which two capacitor plates are formed. If either the top or the bottom (or both) bounding sides of the cavity are made of a flexible ceramic diaphragm, the value of this capacitor will change with pressure. In order to measure this capacitance change, a resonant technique is employed, in which a planar spiral inductor coil fabricated using ceramic-based integral passives techniques is electrically connected to the capacitor. These components form a passive resonant LC circuit, where the resonant frequency is given by[24]:

$$f_o = \frac{1}{2\pi\sqrt{L \bullet C(P)}} \qquad (2)$$

Thus, as the external pressure increases, the capacitance increases and the resonant frequency of the LC circuit will decrease.

To achieve passive wireless telemetry, the circuit is placed in proximity to an external loop antenna coil and the impedance and phase response of the antenna coil are monitored as a function of frequency by an impedance meter. At frequencies far from the sensor frequency (and below the self-resonant frequency of the antenna itself), the antenna appears as an inductance, with a rising impedance response with frequency and a phase shift of +90 degrees. At the sensor resonant frequency, the antenna impedance decreases and the phase response of the antenna drops from +90 degrees.

Although the magnitude of the phase peak depends upon the details of the specific sensor-to-antenna coupling, there are configurations in which the peak position (i.e., frequency) dependencies are negligible. Thus, this wireless data retrieval scheme could also work for a sensor in motion within the antenna (e.g., mounted on a moving part). In addition, it is possible to have an array of such sensors, with each sensor designed to have a distinct 'center' frequency (i.e., frequency given by equation (1) under zero applied pressure), with the number of such sensors limited by the available frequency bandwidth.

Pressure Sensor Design and Fabrication:

The design of the sensor involves the creation of the flexible membrane, the sealed cavity and the integration of the LC resonant circuit. To create the flexible membrane, sealed cavity, and ultimately the capacitor, a multilayer structure is required, see Fig. 15a. A typical sensor is fabricated using 4 sheets of Dupont 951AT ceramic tape[22]. The tape consists of alumina and glass particles suspended in an organic binder. Each sheet is cut to a size of 2.5 inch square with a thickness of ~100μm each. Of the four sheets, two are punched to create the via for the sealed cavity. The diameter of the via is 7.6mm. The four layers are aligned in a press mold that consists of two aluminum plates that are 2.5 inches square and 0.25 inches thick. The ceramic sheets are laminated together in a hot vacuum press for 10 minutes at a press temperature of 70°C and a press force of 9.38 tons under ambient vacuum. After lamination, the sample is cut down to a 1.5 inch square before firing. The sample is fired in a box furnace in air for 30 minutes at 500°C to bake off the organics and then for 20 minutes at 850°C to melt the glass particles and harden the sample.

To create the LC circuit, the top side of the sensor is DC sputtered with an electroplating seed layer of 500Å of titanium followed by 3600Å of copper. Shipley 5740 photoresist is used to create a plating mold that will define the inductor coil and one electrode of the parallel plate capacitor. Using a copper electroplating bath, copper is electroplated onto the seed layer to a thickness of ~28μm and the plating mold and seed layer are removed using wet etching. On the back side of the sensor, the other electrode of the capacitor is patterned using a DC sputtered titanium/copper layer sputtered through a shadow mask. Contact from the outer arm of the inductor coil on the top side of the sensor to the capacitor electrode on the back side is made using Dupont 6160 silver-filled external conductor paste for co-fireable tapes. A diagram of the fabrication process is given in Fig. 15 and a photo-micrograph of a fabricated sensor is given in Fig. 15e.

Sensor Operation:

An antenna coil is placed in the chamber in proximity the sensor and connected to an impedance meter via feedthroughs from a pressure/temperature chamber. The impedance meter reads the phase value of the antenna coil over the frequency range. At atmospheric pressure, the phase of the antenna is +90° except at the resonant frequency of the sensor. At the resonant frequency, the capacitor of the sensor couples to the antenna coil and causes a dip in the phase from +90°. As the chamber pressure increases, the ceramic membrane will deflect causing an increase in the sensor capacitance and a decrease in the resonant frequency and thus, the dip in the phase will shift down in the frequency range.

Wireless pressure and temperature tests were performed using an HP4194A impedance analyzer, a Parr 4570 pressure vessel for high pressure tests, and a VWR vacuum oven for low pressure and temperature tests. Figure 16 shows the raw data obtained, phase versus frequency, for zero and full-scale (1 bar) applied pressure for a single sensor. Figure 18 presents the raw data of Fig. 16 at a variety of pressures between 0 and 1 bar, at 25°C and 200°C. For the results in Figs. 16-17, the pressure sensor was designed to have an electrode radius of 5mm, a membrane thickness of 96μm, and an effective electrode gap of 217μm. The sensitivity of the sensor was calculated from the measured data to be 2.6MHz/bar. The same sensor was tested at 25°C and 200°C and except at low pressures, little difference is seen in sensor performance between the two temperatures. Higher temperatures may have a more significant effect. The highest temperature at which sensors have been successfully tested is currently 400 °C.

Figure 18 illustrates the array concept. Three sensors were tested simultaneously using the same antenna coil. Each sensor was designed for a different center frequency. The variation in peak height for the three sensors reflects different degrees of sensor/antenna coupling (i.e. proximity of the sensor to the antenna coil). However, to determine pressure, only the frequency of the peak is required. Since each sensor has a different carrier frequency and thus a different frequency shift due to pressure, each sensor can be monitored simultaneously by tuning into a particular sensors frequency band.

Acknowledgments

The research described in this paper was supported by AFOSR Contract No. F49620-99-1-0142 (monitored by Dr. Mitat Birkan), DOE/AGTSR Contract No. DE-FC21-92MC29061 (monitored by Dr. Lawrence Golan) and Army MURI Contract No. DAAH04-96-1-0008 (monitored by Dr. David Mann). Special thanks to Dr. Larry Matta who significantly contributed to assembling and editing of the paper. Finally, the authors would like to acknowledge the contributions of graduate students Staci Davis, Jennifer English, Clifford Johnson, Michael Fonseca, Brian Ritchie, Brian Scully, Dilip Mujumdar and Abhijit Kushari to the reported studies.

References

1. Zinn, B. T. and Neumeier, Y., "An Overview of Active Control of Combustion Instabilities," AIAA-97-0461, 35th Aerospace Sciences Meeting and Exhibit, Reno, NV, January 6-9, 1997.
2. Harrje, D. T. and Reardon, F. H., "Liquid Propellant Rocket Combustion Instability," NASA SP-194, 1972.
3. McManus, R. K., Poinsot, T. and Candel, S. M., "A Review of Active Control of Combustion Instabilities," Progress in Energy and Combustion Sciences, Vol. 19, pp. 1-29, 1993.
4. Candel, S. M., "Combustion Instabilities Coupled by Pressure Waves and Their Active Control," 24th Symposium (International) on Combustion, Sydney, Australia, July 1992.
5. Neumier, Y. and Zinn, B. T., "Experimental Demonstration of Active Control of Combustion Instabilities Using Real Time Modes Observation and Secondary Fuel Injections," Proceedings of the 26th International Symposium on Combustion, Naples, Italy, July 28, 1996
6. Johnson, C.E., Neumeier, Y., Lee, J.Y., Neumaier, M. and Zinn, B.T., "Suppression of Combustion Instabilities in a Liquid Fuel Combustor Using a Fast Adaptive Control Algorithm," AIAA-2000-0476, 38th Aerospace Sciences Meeting & Exhibit, Reno, NV, January 10-13, 2000.
7. Zinn, B. T. and Neumeier, Y., United States Patent No. 5,719,791, "Methods, Apparatus and Systems for Real Time Identification and Control of Modes of Oscillations," Feb. 17, 1998
8. Neumeier, Y., Lubarski, E., Heising, R., Israeli, O., Neumaier, M., and Zinn, B. T., "Liquid Injector Actuator for Control of Combustion Instabilities and Processes," 34th AIAA/ASME/SAE/ASEE Joint Propulstion Conf. And Exhibit, Cleveland, OH, July 13-15, 1998..
9. Smith, B. L. and Glezer, A., "Vectoring and Small-Scale Motions Effected in Free Shear Flows using Synthetic Jet Actuators, " AIAA Paper 97-0213.
10. Davis, S. and Glezer, A., "Mixing Control of Fuel Jets Using Synthetic Jet Technology Velocity Field Measurements" AIAA-99-0447, 37th AIAA Aerospace Meeting, Reno, NV, January 1999.
11. Ritchie, B. and Seitzman, J., "Mixing Control of Fuel Jets Using Synthetic Jet Technology Scalar Field Measurements", AIAA-99-0448, 37th AIAA Aerospace Meeting, Reno, NV, January 1999.
12. Chen, Y., Scarborough, D., Liang, S., Aung, K., and Jagoda, J., "Manipulating the Pattern Factor Using Synthetic Jet Actuators," AIAA-2000-1023, 38th Aerospace Sciences Meeting, Reno, NV, January 2000.
13. A. H. Lefebvre, "Fuel Effects on Gas Turbine Combustion – Ignition, Stability and Combustion Efficiency", *ASME J. Eng. Gas Turbines and Power,* vol. 107, pp. 24-37, 1985.
14. K. K. Rink and A. H. Lefebvre, "Pollutant Formation in Heterogeneous Mixtures of Fuel drops and Air", *AIAA J. Propulsion,* vol. 3, No. 1, pp. 5-10, Jan-Feb, 1987.
15. A. Kushari, Y. Neumeier, O. Israeli, A. Peled and B. T. Zinn, "An internally mixed injector for active control of atomization process in liquid fueled engines", AIAA 99-0329, *37th AIAA Aerospace Sciences Meeting and Exhibit*, Jan. 11-14, 1999, Reno, NV.
16. A. Kushari, Y. Neumeier and B. T. Zinn, " A Theoretical Investigation of the Performance of an Internally Mixed Liquid Atomizer", AIAA 2000-1021, *38th AIAA Aerospace Sciences Meeting and Exhibit*, Jan. 2000, Reno, NV.
17. G. Blasquez, P.Pons, and A. Boukabache, "Capabilities and limits of silicon pressure sensors", *Sensors and Actuators*, vol. 17, pp. 387-403.
18. R. Okojie, A. Ned, D. Kurtz, and W. Carr, "6H-SiC pressure sensors for high temperature applications", Proc. MEMS 1996, pp. 146-149.
19. E. Obermermeier, "High Temperature microsensors based on polycrystalline diamond thin films", Proc. International Conf. Transducers '95, pp. 178-181, 1995.
20. Dupont Applied Technologies Group, "Green Tape Material System, Design and Layout Guidelines", pp. 1-17.
21. J. English and M.G. Allen, "Micromachined Wireless Ceramic Pressure Sensors," Proc. IEEE Microelectromechanical Systems Conference, January, 1999.
22. A. Sedra and K. Smith, Microelectronic Circuits, Saunders College Publishing, 1991, pp. 786-788.

Figures

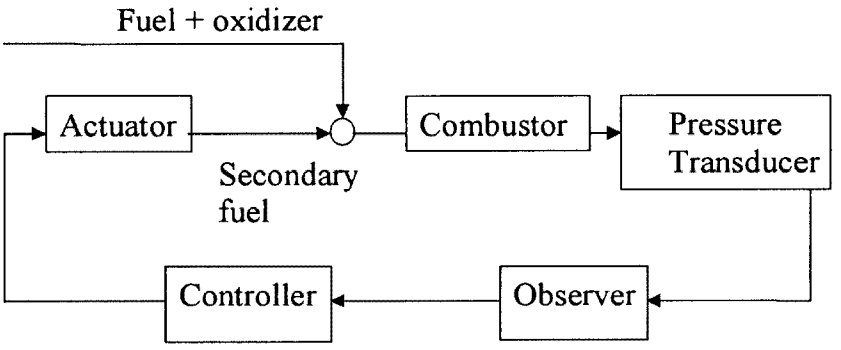

Figure 1. A schematic of the active control system developed at Georgia Tech.

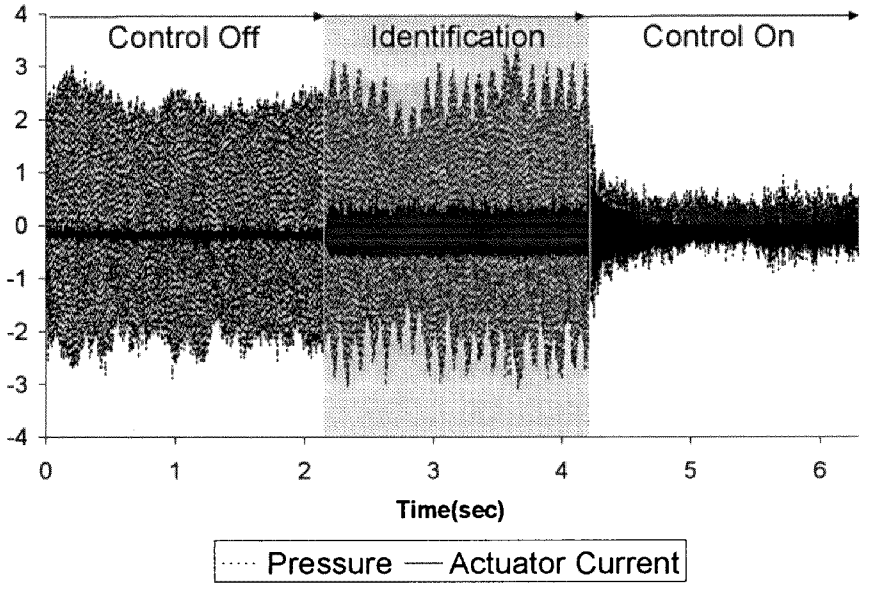

Figure 2. Active adaptive identification and control of combustion instability in the Ga. Tech. combustor (taken from Ref. 6).

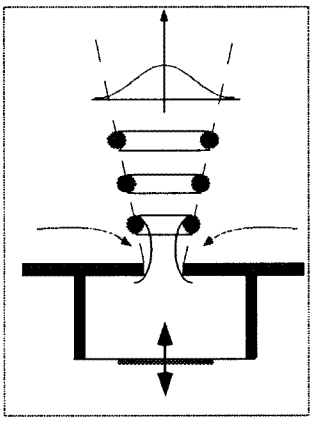

Figure 3. Schematic of a generic synthetic jet actuator.

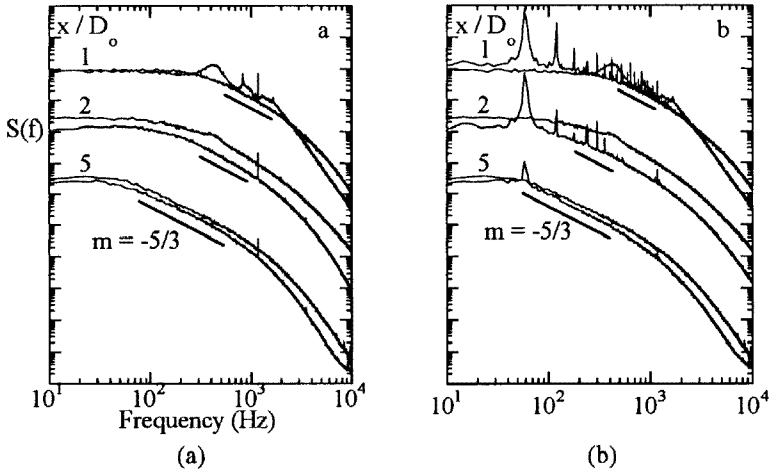

Figure 4. Power spectra of the streamwise velocity at the radial location where $U(x,r) / U_{max}(x) = 0.5$ with $U_i / U_o = 0.65$ for (a) carrier only and (b) amplitude modulated excitation at 60 Hz. Corresponding power spectra of the unforced flow are plotted using gray curves.

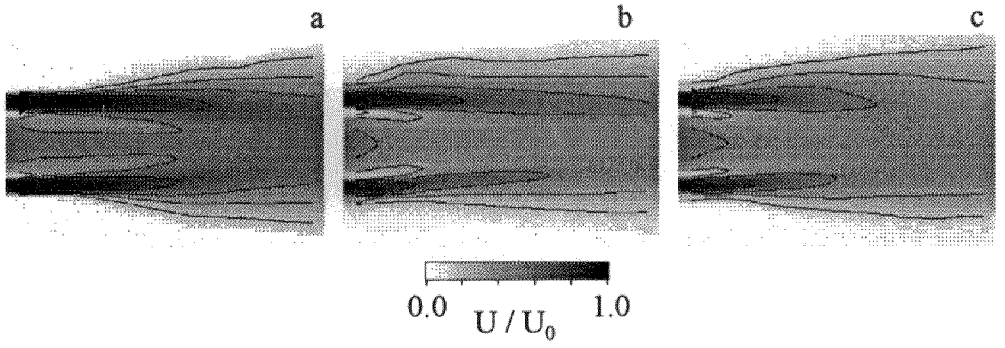

Figure 5. Raster plots of normalized mean streamwise velocity for $U_i / U_o = 0.65$, $x / D_o \leq 3$: (a) unforced, (b) carrier only, and (c) amplitude modulated at 60 Hz. Contours are plotted from 0.2 m/s to 0.8 at intervals of 0.2.

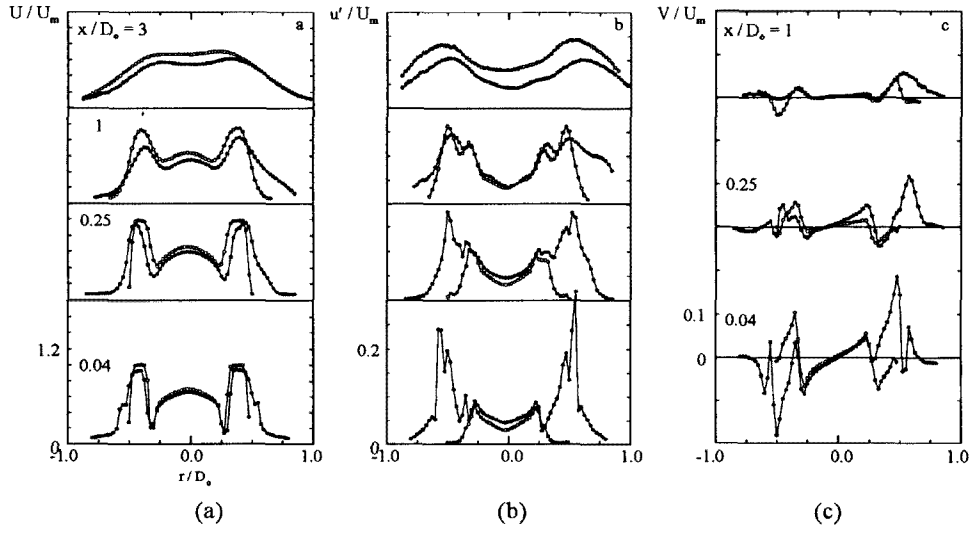

Figure 6. Radial distributions of (a) U, (b) u' , and (c) V for $U_i / U_o = 0.65$: unforced (○), unmodulated forcing.

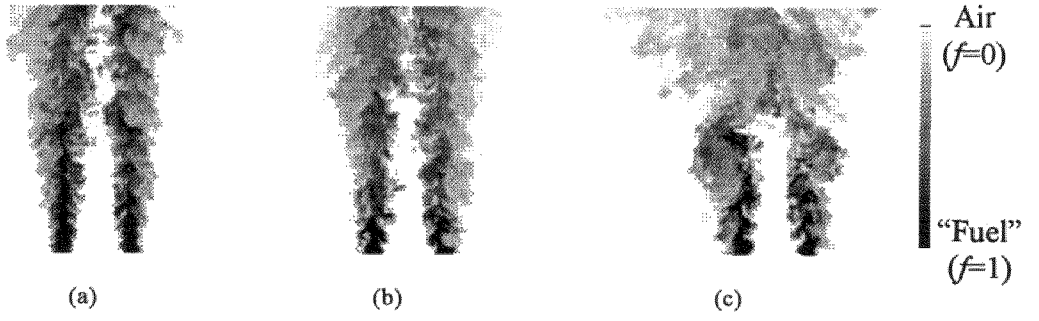

Figure 7. Acetone concentration for $U_i / U_o = 0.65$, $x / D_o \leq 3$: (a) unforced, (b) carrier only, and (c) amplitude modulated at 60Hz.

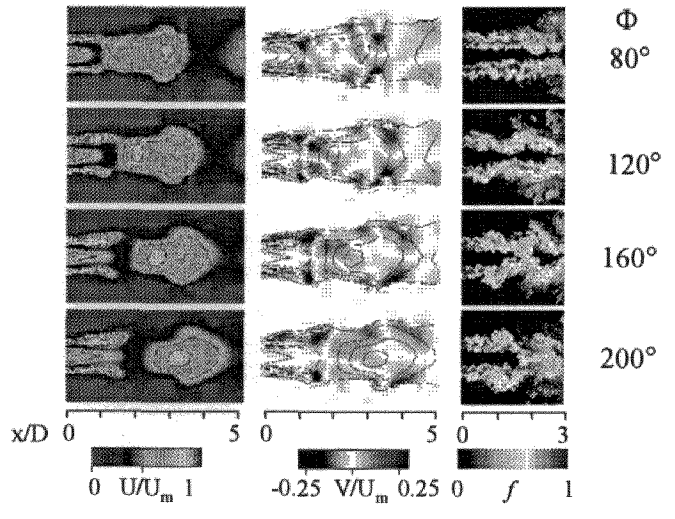

Figure 8. Comparison of velocity (U/U_m = normalized axial velocity, V/U_m = normalized radial velocity) and mixture fraction (f) results for four phases of pulsed forcing and 3 (mixing) or 5 (velocity) diameters downstream.

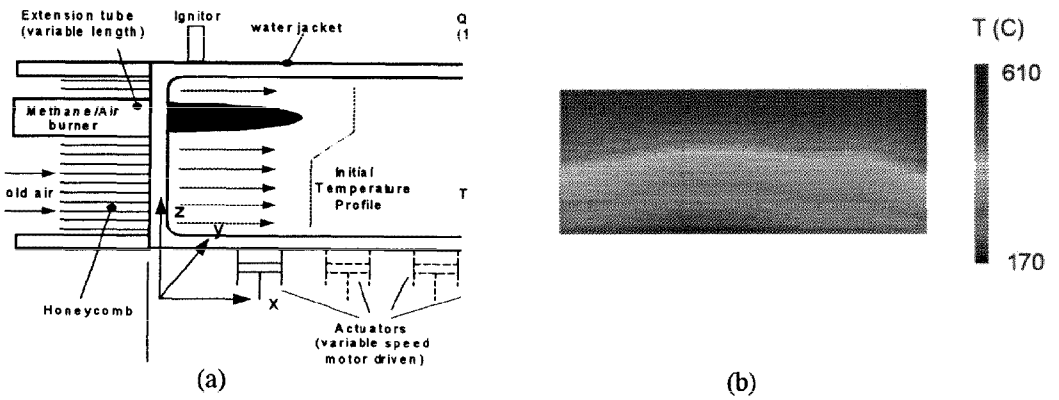

Figure 9. Facility to investigate pattern factor control using SJ – (a) schematic of the setup and (b) typical thermal profile with SJ not activated.

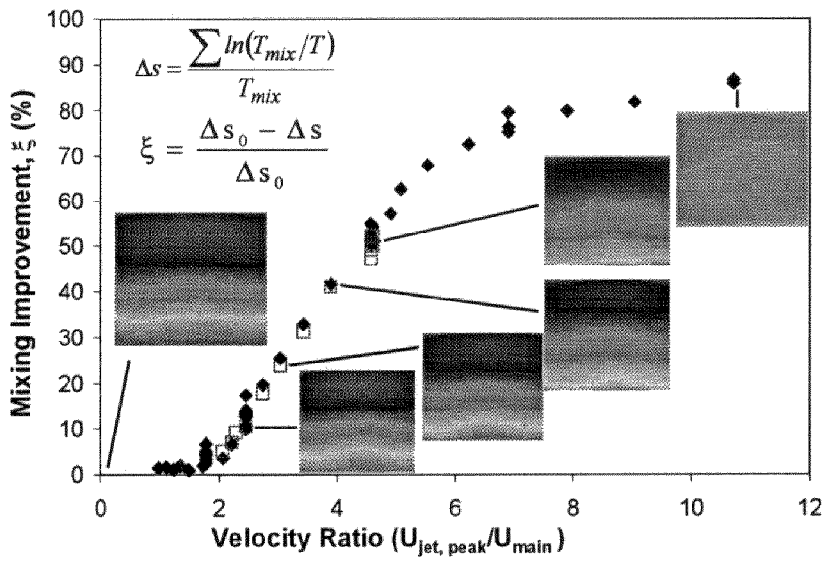

Figure 10. Mixing enhancement due to SJ actuation. Selected temperature profiles are shown to illustrate the mixing improvement.

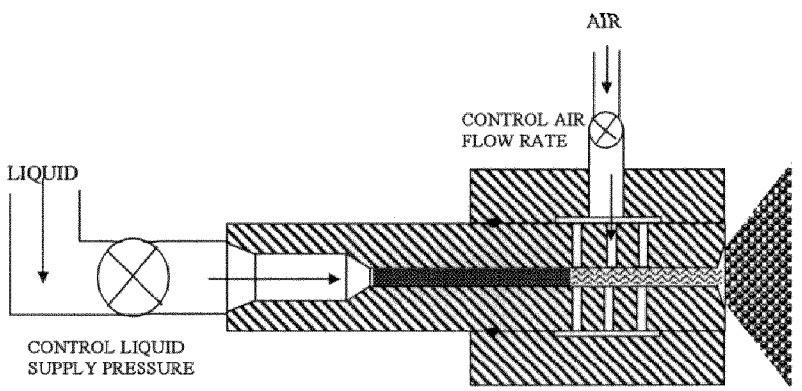

Figure 11: Schematic of the investigated internally mixed atomizer.

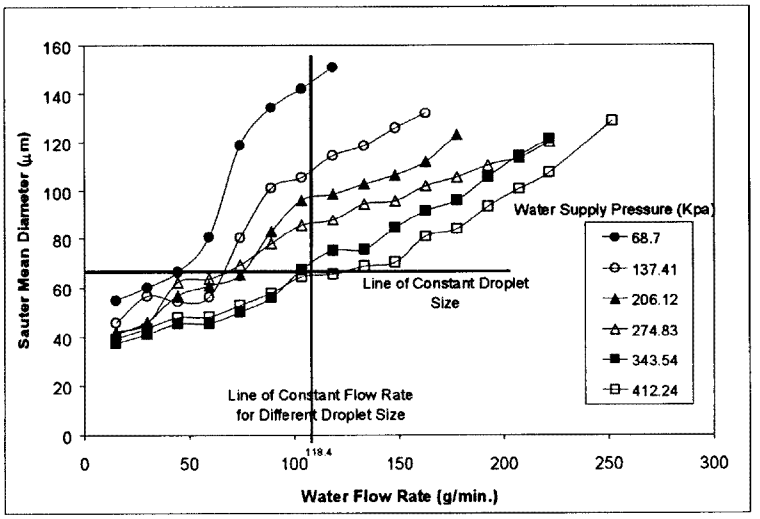

Figure 12: Performance map of the tested atomizer.

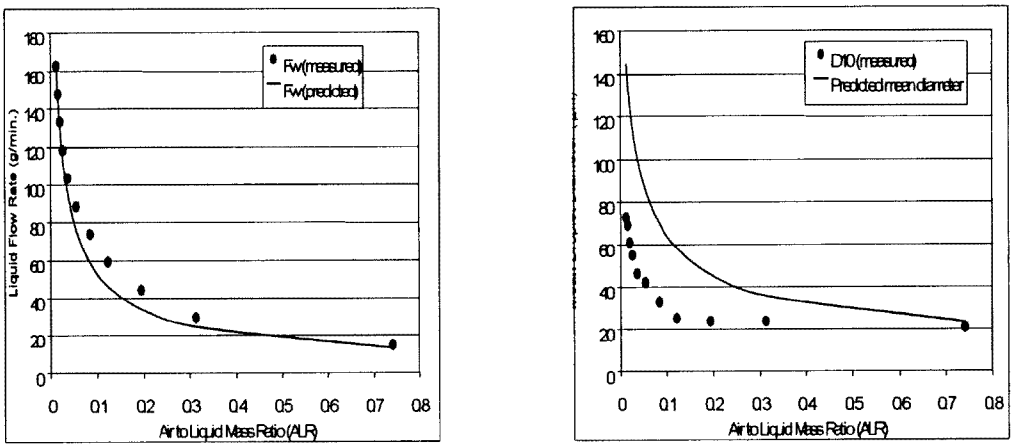

Figure 13. Comparison of theoretical and experimental values of (a) liquid flow rate and (b) drop size.

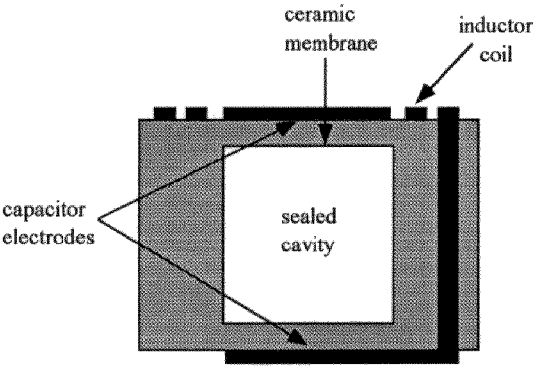

Figure 14. Pressure sensor concept.

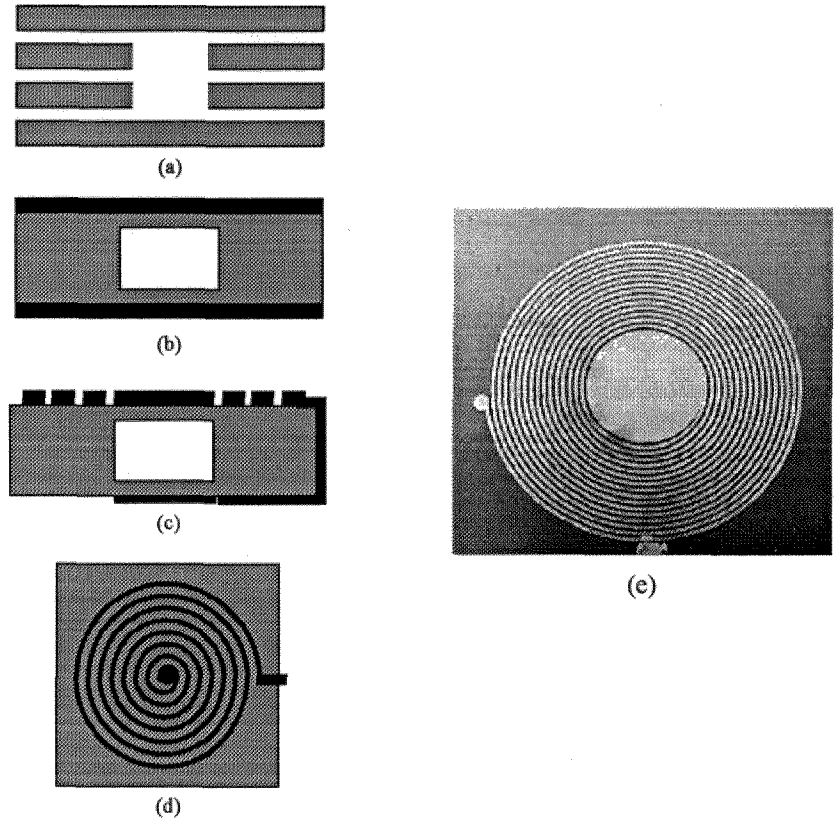

Figure 15. Ceramic micromachined pressure sensor fabrication. (a) ceramic tape layers punched and aligned. (b) after lamination, firing and metallization. (c) after electroplating coil and electrodes. (d) top view of wireless ceramic pressure sensor (e) fabricated sensor.

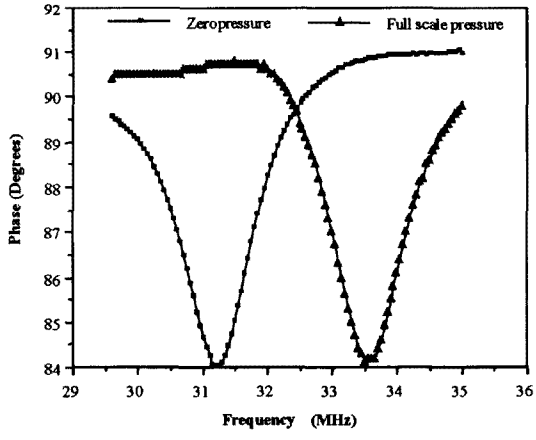

Figure 16. Phase versus frequency for zero and full scale applied pressure (0-1bar).

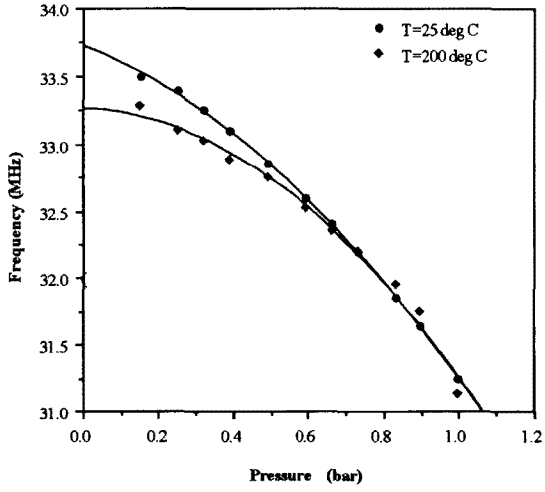

Figure 17. Frequency versus pressure for 25°C (upper curve) and 200°C (0-1bar)

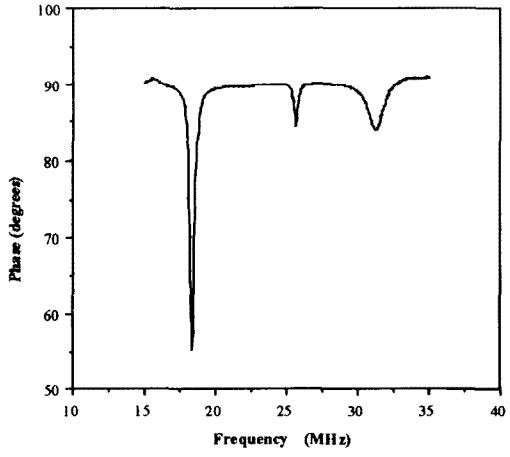

Figure 18. Simultaneous data logged from three sensors within a single loop antenna. Each sensor is designed to have a distinct center frequency, thereby allowing simultaneous readout.

PAPER -6, B. Zinn

Question (A. Annaswamy, USA)

Can you increase the temperature limit to 400-500° C?

Reply

We believe that the higher temperature operation of these sensors could be attained by use of ceramic tapes of different composition. The reported sensors were fabricated from tapes consisting of organic binders, ceramics, and glass. Higher temperature performance could be attained by using available tapes consisting of organic binder and glass only.

Question (D. A. Santavica, USA)

Do you think the synthetic jets will be as effective as your preliminary results show for pattern factor control at typical combustor main flow velocities?

Reply

Synthetic jets have the potential to improve mixing rates within the combustor. Also, they could potentially be used to improve the combustor pattern factor by controlling air/fuel mixing downstream of the burner and the mixing of "hot" and "cold" air pockets downstream of the combustion process. A significant amount of R&D work will be required to achieve these goals.

Question (F. E. C. Culick, USA)

Concerning the missing 2 seconds from the pressure record in your slide (the gap labeled "proprietary"). This is presumably a pressure record faithfully recording what is going on in the chamber. So does the censoring of the tape here mean that the process of system identification in fact interferes with the processes in the chamber?

Reply

The "blacked out" record included descriptions of the measured combustor pressure behavior and control signal to the actuator during the "adaptation" period. These data were omitted on purpose because they are proprietary.